Published in final edited form as:
Invest Ophthalmol Vis Sci. 2009 November ; 50(11): 5226–5237. doi:10.1167/iovs.08-3363.

Scleral Biomechanics in the Aging Monkey Eye

Michaël J. A. Girard[1,2,6], **J-K. Francis Suh**[3,1], **Michael Bottlang**[4], **Claude F. Burgoyne**[5,1], and **J. Crawford Downs**[2,1]

[1] Department of Biomedical Engineering, Tulane University, 6823 St. Charles Avenue, New Orleans LA, 70118

[2] Ocular Biomechanics Laboratory, Devers Eye Institute, 1225 NE 2nd Avenue, Portland, OR 97232

[3] Convergence Technology Laboratory, Korea Institute of Science and Technology, Hawolgok-Dong 39-1, Seongbuk-Gu, Seoul, Korea

[4] Biomechanics Laboratory, Legacy Health Research, 1225 NE 2nd Avenue, Portland, OR 97232

[5] Optic Nerve Head Research Laboratory, Devers Eye Institute, 1225 NE 2nd Avenue, Portland, OR 97232

[6] Current affiliation: Department of Bioengineering, Imperial College London, London UK, SW7 2AZ

Abstract

Purpose—To investigate the age-related differences in the inhomogeneous, anisotropic, nonlinear biomechanical properties of posterior sclera from old (22.9 ± 5.3 years) and young (1.5 ± 0.7 years) rhesus monkeys.

Methods—The posterior scleral shell of each eye was mounted on a custom-built pressurization apparatus, then intraocular pressure (IOP) was elevated from 5 to 45 mmHg while the 3D displacements of the scleral surface were measured using speckle interferometry. Each scleral shell geometry was digitally reconstructed from data generated by a 3D digitizer (topography) and 20 MHz ultrasounds (thickness). An inverse finite element (FE) method incorporating a fiber-reinforced constitutive model was used to extract a unique set of biomechanical properties for each eye. Displacements, thickness, stress, strain, tangent modulus, structural stiffness, and preferred collagen fiber orientation were mapped for each posterior sclera.

Results—The model yielded 3-D deformations of posterior sclera that matched well with those observed experimentally. The posterior sclera exhibited inhomogeneous, anisotropic, nonlinear mechanical behavior. The sclera was significantly thinner ($p = 0.038$), and tangent modulus and structural stiffness were significantly higher in old monkeys ($p < 0.0001$). On average, scleral collagen fibers were circumferentially oriented around the optic nerve head (ONH). We found no difference in the preferred collagen fiber orientation and fiber concentration factor between age groups.

Conclusions—Posterior sclera from old monkeys is significantly stiffer than that from young monkeys and is therefore subject to higher stresses but lower strains at all levels of IOP. Age-related stiffening of the sclera may significantly influence ONH biomechanics, and potentially contribute to age-related susceptibility to glaucomatous vision loss.

J. Crawford Downs, PhD, Ocular Biomechanics Laboratory, Devers Eye Institute, 1225 NE 2nd Avenue, Portland, OR 97232, cdowns@deverseye.org.

Presented in part at the Association for Research in Vision and Ophthalmology annual meeting, Fort Lauderdale, Florida, May 2008.

Commercial relationship: None.

Introduction

Glaucomatous vision loss occurs at both normal and elevated levels of IOP and is the second leading cause of blindness worldwide.[1, 2] The optic nerve head (ONH) has been shown to be the principal site of damage in glaucomatous optic neuropathy,[3, 4] and is a biomechanically compliant tissue in an otherwise strong pressure vessel (the corneo-scleral envelope).[5, 6] While damage to the visual system in glaucoma is multi-factorial, ONH and peripapillary scleral biomechanics provides an overall framework within which the principal pathologic mechanisms in glaucoma can be understood to result in the clinical appearance and behavior of a glaucomatous optic disc.[7, 8]

The ONH contains the lamina cribrosa, a fenestrated connective tissue meshwork that spans the scleral portion of the neural canal and provides structural and functional support to the retinal ganglion cell axons as they exit the eye on their path to the brain. The sclera is the principal load bearing tissue of the eye, and is composed primarily of collagen. Ninety percent of the collagen fibers in the sclera are Type I,[9] which provide the eye with the necessary biomechanical strength to resist IOP. Scleral collagen fibers have a large variation in their diameters[10] and are formed into irregularly arranged, multi-layered lamellae of varying thickness.[11] Within each lamella, the fibrils run tangent to the scleral shell and are oriented in a preferred orientation to varying degrees.[12]

The periphery of the lamina cribrosa inserts deeply into the sclera at the canal wall, and studies have indicated that scleral collagen fiber organization (through idealized models of the monkey eye)[13] and scleral stiffness (through idealized models of the human eye)14 have a large impact on ONH biomechanics. In order to study ONH biomechanics as a potential driving mechanism in glaucoma, computational biomechanical models based on the FE method should incorporate accurate geometries and biomechanical properties for both the ONH and posterior scleral shell.

A variety of data suggest that the human ONH becomes more susceptible to progressive glaucomatous damage as it ages. These data can be summarized as follows. First, in most,[15–19] but not all,[20, 21] population based studies, either IOP does not increase with age or if it does, the magnitude of increase is not likely to be clinically important. Second, normal pressure glaucoma is most commonly a disease of the elderly[22–26] and by most measures exists only rarely in the young.[27] Third, age is an independent risk factor for both the prevalence[28] and progression of the neuropathy at all stages of damage.[29–31]

It is reasonable to hypothesize that age-related changes in ONH biomechanics, blood supply, and other factors may underlie the increased susceptibility to glaucomatous damage in the elderly. There is substantial evidence that the connective tissues of the lamina and sclera are altered with age, which in turn alters their biomechanical behavior. Age-related changes in the human lamina cribrosa have been associated with increased collagen and elastin content as well as increased collagen and elastin cross-links.[32–34] Collagen cross-linking is a characteristic of aging soft-tissues,[35] which result in an increase of stiffness at the tissue or macroscopic level.[36] Several studies using uniaxial tensile testing of scleral strips from tree shrew[37] and human[38–40] eyes concluded that the stiffness of the sclera increases with age.

In this study, we investigate the effects of aging on the biomechanical behavior of posterior sclera obtained from monkey eyes. In recent studies, we reported the 1-D,[41–43] 2-D,[44] and 3-D[45] deformation patterns of posterior and peripapillary sclera using *ex-vivo* experimental protocols. In the present report, we use our latest *ex-vivo* method to experimentally measure the 3-D deformation pattern and thickness of posterior sclera from both eyes of four young and four old monkeys exposed to an experimental IOP elevation from 5 to 45 mmHg.[45] We then model the monkey posterior sclera as a nonlinear, anisotropic, inhomogeneous soft-tissue using a fiber-reinforced constitutive theory that includes stretch-induced stiffening and multi-

directionality of the collagen fiber.[13, 46–50] Finally, we derive eye-specific sets of scleral biomechanical properties based on the experimental observations using an inverse FE method[45], then test the hypothesis that these parameters vary significantly with age.

Material and Methods

Experimental Setup and Testing Protocol

All experiments adhered to the ARVO statement for the Use of Animals in Ophthalmic and Vision Research. Eight rhesus monkeys were included in this study, without any apparent ocular abnormality, classified into two age groups: four were younger than 2.1 years (1.5 ± 0.7 years) and four were older than 18 years (22.9 ± 5.3 years). Note that rhesus monkey age is considered to be approximately one third of human age.[51] For this study, we used an experimental protocol for 3-D scleral testing that has been fully documented in our previous report.13, 45 Briefly, all monkeys were anesthetized with an intramuscular injection of ketamine/xylazine, and sacrificed with an intravenous injection of sodium pentobarbital. The eyes were enucleated immediately after death and all extra-orbital tissues were removed. Each globe was sectioned approximately 3 mm anterior to the equator and the retina and choroid were dissected away from the posterior scleral shell except for a 7-mm diameter patch centered on the ONH, which was left intact to prevent fluid leakage from the ONH during pressurization. After dissection, the posterior scleral shells were individually mounted on a custom-built pressurization apparatus as shown in Figure 1. After mounting, each shell was blotted dry, covered with a contrast medium (ProCAD, Ivoclar, Schaan, Lichtenstein), immediately immersed in isotonic saline at 22°C, and subjected to preconditioning consisting of twenty pressurization cycles from 5 to 15 mm Hg. IOP was incrementally increased from 5 to 45 mmHg and an electronic speckle pattern interferometry sensor52, 53 (Q100, Ettemeyer AG, Germany) was used to record the full-field 3-D displacements of each shell surface at tissue equilibrium. This sensor, consisting of four independent lasers that illuminate the specimen from four directions coupled to a central CCD camera, was operated with a 0.1 μm resolution and was found to generate highly repeatable measurements.52 Finally, displacement components were summed over the following IOP intervals: 5–7, 5–10, 5–20, 5–30, and 5–45 mm Hg. These IOP intervals are within the range experienced during normal activities such as blinking and eye movement and were chosen because they are directly comparable to the *in vivo*, image-based ONH compliance testing and perfusion fixation protocols used in our other monkey studies.54, 55 Following the pressurization experiment, IOP was reset to 5 mmHg and scleral topography was measured with a 3-D digitizer arm (MicroScribe G2X, Immersion, San Jose, CA). Scleral thickness was also measured at twenty predetermined locations: three locations equally spaced between the clamping boundary and the ONH along lines centered in each of the following quadrants: temporal, superior, nasal and inferior; and two locations equally spaced between the clamping boundary and the ONH along lines centered in each of the following quadrants: supero-temporal, supero-nasal, infero-nasal, and infero-temporal). Thickness measurements were made using a 20 MHz ultrasound transducer (PacScan 300P, Sonomed, Inc., Lake Success, NY) with a 1 μm resolution and a measurement reproducibility of less than 4% (data not shown). The topography and thickness data were combined to reconstruct the reference geometry of each posterior scleral shell as shown in Figure 2. The reference geometry was divided into 9 regions, where regions 1–4 encompass the peripheral sclera, regions 5–8 the peripapillary sclera, and region 9 the ONH.

A Constitutive Theory for the Posterior Sclera

In continuum solid mechanics, constitutive theories are developed to mathematically characterize the deformations (strain) and internal forces (stress) of any mechanically loaded material, including biological soft-tissues. As part of our ongoing effort to understand scleral biomechanics and its potential impact on the ONH, we developed a constitutive theory for the

posterior sclera that was validated with experimental observations using electronic speckle pattern interferometry in this study. Our constitutive theory considers collagen – organized into long and dense fibrous bundles – as the primary biomechanical element as it provides most of the tensile strength necessary for the sclera to resist IOP. Accordingly, the posterior sclera is represented as a fiber-reinforced composite structure, in which the collagen fibers are (1) responsible for two important biomechanical characteristics (anisotropy and nonlinearity) and (2) embedded within a ground substance matrix. The following is a brief summary of our constitutive theory, which is fully described in our previous report.[13, 45]

Anisotropy—Anisotropy, as opposed to isotropy, is the property by which materials exhibit different stiffnesses along different orientations. Anisotropy in thin soft tissues is generally determined by the organization of their collagen fibers, which run tangent to the tissue surface in the sclera.[12] We used a semi-circular von-Mises distribution[56] to describe planar anisotropy of the posterior sclera, in which θ_p is an angle that defines the preferred fiber orientation and k is the fiber concentration factor (Figure 3). Figure 3 illustrates the different degrees of collagen fiber alignment for varying k values and $\theta_p = 0°$ described by this distribution. When $k = 0$, the fibers are unorganized and their orientations are random (planar isotropy). As k increases, the fibers become increasingly more aligned along the preferred fiber orientation, θ_p, and hence more stiff in that direction, resulting in anisotropy.

Nonlinearity—Collagen fibers uncrimp with stretch,[57] which results in tissues that are initially compliant at low stretch but increase in stiffness at higher levels of stretch (Figure 4). This property is known as nonlinearity and has been experimentally observed in the posterior sclera.[36, 37, 39, 44, 45, 58–63] An increase of stiffness is known to protect soft-tissues from undergoing large deformations, which could disrupt the tissue's mechanical integrity at the cellular level.[39] For our constitutive theory, IOP-induced stiffening of the sclera is described by specifying the collagen fiber stress as an exponential function of the collagen fiber stretch. Within this relationship, two model parameters govern the degree of nonlinearity of the posterior sclera (c_3: exponential fiber stress coefficient, and c_4: uncrimping rate of the collagen fibers).[13, 64] Note that the product of c_3 and c_4 dominates the scleral response at low IOP, but c_4 alone dominates the scleral response at high IOP.

Ground Substance Matrix—In our formulation, the ground substance matrix – not to be confused with the extracellular matrix – contains all non-collagenous tissue components (*e.g.* elastin, glycosaminoglycans, proteoglycans, fibroblasts, tissue fluid). The ground substance matrix is assumed to be isotropic, and hence its mechanical behavior can be described with a single intrinsic model parameter (c_1, the 1st Mooney-Rivlin coefficient).[13, 64]

Model Assumptions

The model assumed that stiffness of the ground substance matrix (c_1) and the nonlinear stiffness of the collagen fibers (c_3, c_4) were uniformly attributed to the entire scleral shell (Regions 1–8; Figure 2). It further assumed that regional variations of the scleral biomechanical response were governed by the local alignment of the collagen fibers. Accordingly, fiber concentration factors, k_1 and k_2, were attributed to the peripheral sclera (Regions 1–4; Figure 2) and to the peripapillary sclera (Regions 5–8; Figure 2), respectively. Finally, a total of eight preferred fiber orientations, θ_{p1} to θ_{p8}, were attributed to each of the eight scleral regions, respectively (Figure 2). Two studies have suggested that the mechanical properties of the ONH have a limited impact on scleral biomechanics,[14, 45] so the ONH was modeled as linear elastic and incompressible with an elastic modulus of 1 MPa for all eyes.

Estimation of Model Parameters: Inverse Finite Element (FE) Method

For each posterior scleral shell, we estimated a set of thirteen model parameters (c_1, c_3, c_4, k_1, k_2, θ_{p1} to θ_{p8}) from the experimental data using an inverse FE method that is described in our previous report.45 Briefly, the inverse FE method allows the thirteen model parameters to be determined from the experimentally-measured displacements by simultaneously varying their values until the FE-computed displacements (x, y, and z) closely match the experimentally-measured displacements for all IOP levels (7, 10, 20, 30 and 45 mmHg). The inverse FE method is driven by a genetic optimization algorithm (differential evolution65, 66) and yields a unique set of thirteen model parameters for each scleral shell.45 Agreement between the FE-computed and experimentally-measured displacements was evaluated according to an error criterion defined in our previous study, which compares the 3D displacement at each node in the FE model to the equivalent location in the experimental pressurization tests.45

Additional Measures of Scleral Stiffness

Tangent modulus—The model parameters c_3 and c_4 describe the stretch-induced stiffening of the collagen fibers, but do not represent a direct measure of scleral stiffness at each IOP. To capture scleral tissue stiffness, two additional quantities were calculated and mapped: the tangent modulus along the preferred fiber orientation and the tangent modulus perpendicular to the preferred fiber orientation. Both tangent moduli represent estimates of local scleral tissue stiffness (a bulk tissue property), can be computed at each IOP, and are functions of the model parameters and the local collagen fiber stretch.[45]

Structural stiffness—Clinical discussions concerning the observable mechanical behavior of the corneo-scleral shell often confuse the separate contributions of the tissues' biomechanical properties and their geometry. We calculated and continuously mapped structural stiffness – defined as the product of local scleral thickness and local values for each tangent modulus – to capture the mechanical behavior of the scleral shell as a structure in response to acute IOP elevations.

Statistical Analysis

Regional distributions of tangent moduli and structural stiffnesses were compared between age groups (young and old) for both the peripapillary and peripheral sclera using the generalized estimating equation method. Thickness measurements were compared between age groups using a multiple linear regression.

Results

The derived model parameters (except the eight preferred fiber orientations), as well as monkey age and sex information are reported in Table 1 for each eye. The maps of scleral thickness, experimentally-measured and FE-computed displacements, tangent modulus, structural stiffness, maximum principal stress and strain, and the eight derived preferred fiber orientations are presented in Figure 5 for each eye. The pooled distributions of preferred fiber orientation are shown in Figure 6. Finally, the pooled distributions (25^{th}, 50^{th} and 75^{th} percentiles) of maximum principal stress and strain as well as tangent moduli are presented in Figure 7.

Results Common to all Eyes and Monkeys

Scleral thickness, experimentally measured at an IOP of 5 mmHg at twenty locations and interpolated over each scleral shell, is shown in Figure 5 (first row). In all eyes, the peripapillary sclera was much thicker than the peripheral sclera. Among all regions (*i.e.* inferior, infero-

nasal, nasal, supero-nasal, superior, supero-temporal, temporal, infero-temporal), the sclera was considerably thicker in the temporal region for all sixteen eyes ($p < 0.0001$).

For each eye, good agreement (according to a criterion defined in our previous study)[45] was obtained between FE-computed and experimentally-measured displacements at all IOPs (second and third rows of Figure 5). Fitting error averaged less than 4.92 μm in all sixteen eyes. Figure 5 also shows that the results obtained for the two eyes of each monkey are remarkably similar for all measures, but vary more substantially between monkeys.

Regional variations (inhomogeneity) in tangent modulus and structural stiffness along the preferred fiber orientation, and in maximum principal strain and stress at an IOP of 30 mmHg were present and consistent within the eyes of each monkey (Figure 5). In all eyes, we observed that tangent modulus was higher in the peripheral sclera than in the peripapillary sclera, which suggests that tangent modulus is inversely related to scleral thickness. As a result, the structural stiffness, the local product of the tangent modulus and scleral thickness, was more uniformly distributed when compared to scleral thickness and tangent modulus. From Figure 5, we consistently observed tangent modulus, structural stiffness, strain and stress concentrations near the scleral canal.

Maps of the derived preferred fiber orientation for all eight regions of each eye are shown in Figure 5, where ⊥ (white) indicates a preferred fiber orientation perpendicular to the scleral canal, and // (black) a preferred fiber orientation tangent to the scleral canal. Figure 6 shows the pooled distributions of the preferred fiber orientation for all sixteen eyes in both the peripapillary and peripheral sclera. In general, the mean preferred fiber orientation for all tested eyes was tangent to the scleral canal in both scleral regions.

Separate from the above results, the fiber concentration factor in the peripapillary sclera (k_2) was higher than that in the peripheral sclera (k_1) for fourteen of the sixteen eyes studied (Table 1). This result suggests that the collagen fibers are more aligned along the preferred fiber orientation (as explained in Figure 3) in the peripapillary sclera compared to the peripheral sclera. Note that non-zero fiber concentration factors suggest that the sclera is anisotropic (Figure 3).

Overall distributions of the tangent moduli in both the peripapillary and peripheral sclera are shown on Figure 7. Tangent moduli dramatically increased from 5 to 45 mmHg in both regions of all scleral shells. This finding confirms that the posterior sclera is highly nonlinear and stiffens as IOP increases. Also note that the tangent moduli were higher in the thin peripheral sclera than in the thick peripapillary sclera. In all eyes, maximum principal strain (a local measure of tensile deformation) was a nonlinear function of IOP and relatively low even at an IOP of 45 mmHg, averaging 1.1% and 0.5% in the peripapillary sclera from young and old monkeys, respectively. Maximum principal stress (a local measure of internal forces) was a linear function of IOP and considerably higher than IOP, averaging 17 and 24 × IOP in the peripapillary sclera from young and old monkeys, respectively.

Age-related changes in scleral biomechanics

Using a multiple linear regression, we found that the posterior sclera was significantly thinner overall ($p = 0.038$) in the eyes from old monkeys compared to that from young monkeys. In the peripapillary sclera, thickness measurements averaged 349 ± 49.5 μm and 389 ± 53 μm in old and young eyes, respectively. Thickness measurements in the peripheral sclera averaged 173 ± 44 μm and 239 ± 49 μm in old and young eyes, respectively.

The parameters c_1 and c_4 (Table 1) were generally higher in the eyes from the old monkeys, which suggests that the aged eyes have a stiffer ground substance matrix and a higher collagen

fiber uncrimping rate (*i.e.* the fibers stiffen more quickly as IOP increases) than eyes from younger monkeys. Accordingly, the scleral tangent moduli from old monkeys increased by a factor of approximately 7 to 8 for IOPs from 5 to 45 mmHg, compared to a factor of approximately 4 to 5 in sclera from young monkeys (Figure 7). Scleral tangent moduli and structural stiffnesses (along and perpendicular to the preferred fiber orientation) were significantly higher for the old monkey eyes in both the peripheral and peripapillary sclera at all levels of IOP ($p < 0.001$ for all comparisons). Figure 7 also shows that posterior sclera from old monkeys exhibited less strain but higher stress than that from young monkeys at all levels of IOP for both the peripheral and peripapillary sclera regions. Note that although our results show that young monkeys exhibited significantly lower scleral tangent moduli and structural stiffnesses, one pair of eyes (monkey 2) was in the same range as the old group (Figure 5).

We did not detect age-related changes in the fiber concentration factor ($p > 0.05$) or in the preferred fiber orientation ($p > 0.05$) in any regions.

Discussion

In this report, we measured the 3-D displacements of the posterior scleral shell from both eyes of 4 young and 4 old monkeys exposed to acute elevations of IOP from 5 to 45 mmHg, and estimated inhomogeneous, anisotropic, nonlinear biomechanical properties for each individual shell using an inverse FE method. Our principal findings are as follows. First, peripapillary and posterior sclera is significantly thinner in aged eyes. Second, monkey sclera is a highly nonlinear, anisotropic, and inhomogeneous soft-tissue. Third, inverse FE simulations predicted that collagen fibers were, on average, circumferentially oriented around the scleral canal in both the peripapillary and peripheral sclera (Figure 6), as well as more aligned along the preferred fiber orientation in the peripapillary sclera (Table 1). Fourth, monkey peripapillary and posterior sclera stiffens significantly with age by all measures considered in this study. Fifth, peripapillary concentrations of tangent modulus, structural stiffness, strain and stress (adjacent to the scleral canal) were present at high IOP in each eye. Sixth, apart from their concentrations, the magnitude of scleral stress was substantially higher than IOP at all levels of IOP. Seventh, the magnitude of strain in the peripapillary and posterior sclera of both the young and old eyes was surprisingly low.

On average, the sclera was thickest in the peripapillary region overall and in the temporal region specifically (Figure 5), which is in agreement with our previous study on thickness characterization of monkey posterior sclera using traditional histology.[67] We also observed a significant thinning of the sclera with age ($p = 0.038$). While scleral thickness is sure to increase during the first few months of development associated with eye growth, information regarding the change of scleral thickness with age at later stages of life remains controversial. In humans, some investigators have reported an increase of scleral thickness with age,[12, 38] while others reported[68] or suggested[69] a decreasing trend. In tree shrews, scleral thickness was shown to be stable between 1 and 24 months of age.[70] Further studies in non-human primates should be conducted in order to validate our result.

Figure 7 shows that monkey posterior sclera exhibited a highly nonlinear response to acute IOP elevation from 5 to 45 mmHg as demonstrated by the dramatic increase in tangent moduli with IOP. This behavior was observed in all eyes in both age groups, and has been previously reported by our group in porcine sclera,44 and by others in human sclera.[58] Interestingly, the rate of scleral stiffening with IOP was higher in the posterior sclera from old monkeys (7 to 8 fold) compared to that from young monkeys (4 to 5 fold). This finding suggests that aged eyes will exhibit a larger stress increase with transient IOP elevations than younger eyes. It remains to be determined if transient increases in stress or strain will correlate with tissue damage or

remodeling. The accumulated exposure to IOP spikes over a period of years may contribute to age-related glaucomatous susceptibility, which has been proposed previously.[71, 72]

Monkey posterior sclera is highly anisotropic and inhomogeneous, which manifests most prominently as non-zero fiber concentration factors (Table 1) and as inhomogeneous tangent modulus fields (Figure 5). It is interesting to note that as a mechanical structure, structural stiffness is more homogeneous than either scleral thickness or tangent modulus. This indicates that these eyes are likely to expand relatively uniformly as IOP increases, and that the eye's mechanical response is optimized to maintain the constant retinal curvature necessary for focused vision.

In all eyes, inverse FE simulations predicted that the collagen fibers were, on average, circumferentially oriented around the scleral canal in both the peripapillary and peripheral sclera (Figure 6), which is consistent with previous histologic results for the peripapillary sclera[73, 74]. Moreover, in 14 of 16 eyes, the collagen fibers tended to be more highly aligned along their preferred orientations in the peripapillary sclera compared with the peripheral sclera as shown by the higher peripapillary fiber concentration factor (k_2; Table 1). Our previous computational study of posterior scleral biomechanics suggests that the presence of highly aligned, circumferential fibers in the peripapillary sclera reduces IOP-induced scleral canal expansion considerably[13], and this arrangement may be biologically optimized to protect the contained ONH from biomechanical damage.

Although sclera was thinner in old monkey eyes, their tangent moduli were higher, and the resulting structural stiffness was higher than that measured in young monkey eyes ($p < 0.001$). Aging effects were measured in all parameters, in which posterior sclera from old eyes was thinner, yet exhibited significantly higher tangent moduli and structural stiffness compared to eyes from young monkeys. The older monkeys also exhibited higher scleral stress but lower strain than the young monkeys.

In all eyes, we observed high tangent modulus, structural stiffness, strain and stress at the scleral canal boundary. Stress within the peripapillary sclera was considerably higher than IOP at all IOP levels, averaging 17 and 24 × IOP but rising as high as 24 and 32 × IOP in the 75th percentiles for young and old monkeys, respectively. These stress values are significantly higher than those initial hypothesized by Greene and coworkers75 and comparable to the ranges reported by Bellezza and coworkers5 (11 to 27 × IOP in the peripapillary sclera) and by Sigal and coworkers[6] (9 to 12 × IOP in the posterior sclera) in idealized FE models of the human eye. Unlike previous studies, the reported stress estimates were obtained based on anatomically accurate posterior scleral geometries, 3-D experimental deformation measurements, and a more realistic constitutive theory, and are therefore likely to be the most accurate estimates for the monkey eye to date.

Our reported strain values were consistently low (2.4% was the highest peak strain detected) as opposed to strains experienced by other thin collagenous soft-tissues such as arteries and ligaments.[76, 77] A variety of previous studies have reported that mechanical strain on scleral fibroblasts resulted in the suppression of TIMP-1 (0.45% cyclic strain in humans78), in changes in gene expression (4% constant strain in humans79), in the production of MMP-2 and suppression of TIMP-2 (15% cyclic strain in humans80), and in enhanced expression of both MMP-2 and TIMP-2 mRNA (20% cyclic strain in chicks81). According to these studies, a wide range of strain levels has the capacity to trigger remodeling of the scleral extracellular matrix, which could result in scleral thinning or thickening, and/or scleral softening or stiffening. It will become important that future experimental studies on scleral cell and tissue biomechanics consider the levels of strain that we report, as the higher levels often used in cellular work may be nonphysiologic.

Considered together, the results of this study raise important clinical questions regarding the role of age-related peripapillary and posterior scleral stiffening in the susceptibility to glaucomatous damage and clinical behavior of the aged eye.71 In simple terms and if all other components of ONH biomechanics are equal, an isolated increase in scleral stiffness should considerably limit scleral canal expansion, which prevents the lamina cribrosa from being pulled taut at elevated IOP. As scleral canal expansion and posterior laminar deformations are likely to be inversely related (described in our previous computational study13), the lamina cribrosa associated with a stiffer sclera should undergo larger posterior deformation at all levels of IOP due to the direct action of IOP on the ONH surface. How a similar age-related increase in lamina cribrosa connective tissues stiffness[32–34, 82–86] affects this scenario is unknown.

In general, for a given magnitude of IOP insult, the aged ONH should demonstrate less deformation due to the presence of a stiffer lamina and a stiffer peripapillary sclera. But as can be seen by the above discussion, the effects of scleral stiffness alone, without knowing the biomechanical properties or behavior of the lamina, will be difficult to predict. Whether a stiff sclera is always associated with a stiff lamina and whether a stiff lamina is more or less prone to axon loss for a given form of IOP insult, are core issues in the study of ONH susceptibility. We are currently using biomechanical FE modeling to study the interactions between scleral and ONH biomechanics and their contributions to the susceptibility of the aged monkey and human eye. This work will be the topic of future reports.

Several limitations should be considered when viewing this work. While the general limitations of the method have been discussed at length in our previous reports.[13, 45] we briefly revisit them here and focus only on those inherent to this study. First, all experiments were conducted at a nonphysiological temperature (22 °C instead of 37 °C). Curtin39 and Greene and coworkers87 studied the effect of temperature on scleral biomechanics. Curtin found no consistent effects of temperature upon the stress response of sclera between 37 and 41 °C and Greene found that scleral creep rates were greatly impacted by temperature. In tendons and ligaments (tissues that are very similar to sclera in composition), Rigby and coworkers88 have found that temperature has no effect on their mechanical behavior between 0 and 37 °C, but the mechanical behavior can change dramatically above 37 °C. On the contrary, Woo and coworkers89 found that temperature has a large impact on the mechanical behavior of ligaments between 2 and 37 °C. While convincing data regarding the effects of temperature on scleral biomechanics are not available, we do not disregard the fact that temperature could have an impact on the mechanical behavior of the posterior sclera and the ONH tissues in general. Due the extremely high resolution of our speckle interferometry sensor (0.1 μm), we could not use a 37 °C heating chamber because mechanical disturbances arising from thermal expansion/contraction of the pressurization apparatus and fluid convection within the saline chamber greatly affect the scleral surface displacement measurements. Because all experiments were consistently performed at room temperature, our ability to test for differences between both age groups should not be affected. Whether our material property estimates accurately reflect those at 37 °C needs to be determined.

Second, we have assumed that collagen was the primary fibrous element of the sclera,[57] and we have lumped all other tissue constituents into the ground substance matrix. This is a common practice in soft-tissue FE modeling.[64, 90] As such, our formulation assumes that inhomogeneity of the sclera is solely dependent on the orientation of the collagen fibers. We have therefore ignored the regional-variations in collagen fiber diameter and elastin content that are known to exist in human posterior sclera (*e.g.* relatively large collagen fiber diameter and almost no elastin in the peripheral sclera of human eyes)[10] as well as the potential contribution of elastin to tissue anisotropy.[91] Adding such information to a constitutive theory is not a straightforward task and further experimental and theoretical work will be needed to address how these

components influence scleral biomechanics. However, these limitations should not alter the results or conclusions of this study.

Third, we did not characterize scleral biomechanics between 0 and 5 mmHg in the tested eyes because the scleral shells required an IOP of approximately 4 mmHg to sustain their shape. The inherent 'floppiness' of monkey sclera is an indication that residual scleral stress is minimal and can be neglected. IOPs in the range of 0–5 mmHg are rarely measured in monkey eyes, so ignoring the initial IOP loading should not compromise the importance of our results.

Fourth, the ONH tissues were assumed to be linearly elastic, with a common elastic modulus of 1 MPa assigned to the ONH region for both young and old monkey eyes. As previously mentioned, evidence suggests that ONH tissues, especially the lamina cribrosa, become stiffer with age and therefore we could have assigned a lower elastic modulus for the younger eyes. In the absence of reported data on age-dependent laminar moduli in monkeys, we felt it was more conservative to assign a common laminar modulus to all eyes to facilitate comparison of scleral biomechanics between age groups. Our previous sensitivity study showed that ONH elastic moduli in the range of 0.1–5 MPa did not affect the results of our scleral biomechanical property fitting.[45] This agrees with several studies that have shown that ONH biomechanics has only a slight impact on scleral biomechanics[6, 13, 14], although the inverse is untrue. Hence, our assumption of using the same ONH modulus for both young and old eyes should not impact the results presented herein.

Fifth, the ONH was represented as an elliptical cylinder, with its external boundary located at the outer aspect of the dural sheath insertion (as measured with the 3-D digitizer) and was therefore larger than one would expect (~2 mm along the major axis in our model, compared with ~1.5 mm for an anatomic ONH). A better characterization of ONH biomechanics that incorporates accurate ONH geometries and inhomogeneous, anisotropic biomechanical properties is currently underway in our laboratory.[92, 93] When combined with the present work on scleral biomechanics, we should gain an enhanced understanding of the complex interactions between scleral and ONH biomechanics.

Sixth, we divided each reconstructed scleral shell into eight regions to estimate regional variations in collagen fiber orientation (θ_{p1} to θ_{p8}). Specifying more regions, and therefore more model parameters, would dramatically increase the computational time required for each inverse FE simulation and raise concerns about solution uniqueness. Our preliminary study confirmed that a combination of eight regions and thirteen model parameters was the minimum requirement to obtain good agreement between the FE-computed and experimentally-measured displacements (Figure 5) while also ensuring a unique set of model parameters for each eye (data not shown). Note that dividing the posterior sclera into eight regions resulted in strain, stress, tangent modulus, and structural stiffness discontinuities in the vicinity of the regional boundaries (Figure 5). This limits accuracy of the models at those boundaries and introduces artificially high stress and strain in those areas. We were careful to ignore these artificially high values in the presentation of results in Figure 7, in which we reported the 25th, 50th, and 75th percentile values of each parameter.

Seventh, collagen fiber alignment was not measured directly, but was derived using the models' fits to experimentally-measured scleral deformations (Figure 5). Due to the relatively coarse discretization of the regions (discussed above) we could only report an overall approximation of the preferred collagen fiber orientation within each region. However, our averaged results appear consistent with previous histologic findings showing that collagen fibers are highly aligned and organized into a circumferential ring around the scleral canal,[73, 74, 94] and that collagen fibers from the peripheral sclera are more irregularly arranged to form interwoven lamellae.[11, 12, 95] Future inclusion of experimentally-derived collagen fiber orientation maps

as an input parameter will allow for finer regional discretization for the remaining fitted parameters, and improve our characterization of scleral anisotropy.

Finally, viscoelastic effects were not considered in this study for several reasons. 1) We have previously characterized the viscoelastic behavior of monkey and rabbit peripapillary sclera.[41–43] 2) Our displacement sensor requires approximately four seconds to acquire data for each loading step, which is not fast enough to adequately capture time-dependent displacements. 3) While viscoelasticity plays a role in the eye's response to IOP fluctuations, it is currently unknown if the viscous behavior of the posterior sclera is important in the development of chronic diseases such as glaucoma. 4) Combining anisotropic, nonlinear and viscoelastic mechanical behaviors is a complex task and we have chosen to limit ourselves to anisotropic and nonlinear behaviors in this investigation. Ultimately, we would like to combine those three mechanical phenomena in our future models of the eye.

In summary, new experimental and computational methodologies[13, 45] have been applied to the study of scleral biomechanics in the aging monkey eye. These methods can be applied to other thin soft tissues with multi-directional collagen fibers and will now be used to characterize scleral biomechanics in glaucomatous monkey eyes. Given that human and monkey posterior sclera have similar organic compositions and metabolism, although slight differences are known to exist,[10] human sclera should exhibit similar biomechanical changes with age. This will be confirmed in a future study of scleral biomechanics in the aging human eye. The long-term goal of our work is to establish the pathophysiologic links between connective tissue stress/strain within the peripapillary sclera and lamina cribrosa and retinal ganglion cell axon damage and death. Given the determining role of scleral biomechanics on both the neural and connective tissues of the ONH, new strategies for the clinical study (visualization and measurement) of peripapillary and posterior scleral biomechanics are indicated.

Acknowledgments

This work was supported by the NIH (RO1EY11610; CFB) and the Legacy Good Samaritan Foundation, Portland, Oregon. The authors wish to thank Juan Reynaud, Jonathan Grimm, Wenxia Wang, and Stuart Gardiner for their contributions to this work.

References

1. Resnikoff S, Pascolini D, Etya'ale D, et al. Global data on visual impairment in the year 2002. Bull World Health Organ 2004;82:844–851. [PubMed: 15640920]
2. Foster A, Resnikoff S. The impact of Vision 2020 on global blindness. Eye 2005;19:1133–1135. [PubMed: 16304595]
3. Quigley H, Anderson DR. The dynamics and location of axonal transport blockade by acute intraocular pressure elevation in primate optic nerve. Invest Ophthalmol 1976;15:606–616. [PubMed: 60300]
4. Quigley HA, Addicks EM. Chronic experimental glaucoma in primates. II. Effect of extended intraocular pressure elevation on optic nerve head and axonal transport. Invest Ophthalmol Vis Sci 1980;19:137–152. [PubMed: 6153173]
5. Bellezza AJ, Hart RT, Burgoyne CF. The optic nerve head as a biomechanical structure: initial finite element modeling. Invest Ophthalmol Vis Sci 2000;41:2991–3000. [PubMed: 10967056]
6. Sigal IA, Flanagan JG, Tertinegg I, Ethier CR. Finite element modeling of optic nerve head biomechanics. Invest Ophthalmol Vis Sci 2004;45:4378–4387. [PubMed: 15557446]
7. Burgoyne CF, Downs JC, Bellezza AJ, Suh JK, Hart RT. The optic nerve head as a biomechanical structure: a new paradigm for understanding the role of IOP-related stress and strain in the pathophysiology of glaucomatous optic nerve head damage. Prog Retin Eye Res 2005;24:39–73. [PubMed: 15555526]
8. Ethier CR. Scleral biomechanics and glaucoma--a connection? Can J Ophthalmol 2006;41:9–12. 14. [PubMed: 16462866]

9. Edelhauser, HF.; Ubels, JL. Adler's physiology of the eye, Clinical applications. St. Louis, Missouri: Mosby; 2003. The cornea and the sclera.
10. Quigley HA, Dorman-Pease ME, Brown AE. Quantitative study of collagen and elastin of the optic nerve head and sclera in human and experimental monkey glaucoma. Curr Eye Res 1991;10:877–888. [PubMed: 1790718]
11. Rada JA, Shelton S, Norton TT. The sclera and myopia. Exp Eye Res 2006;82:185–200. [PubMed: 16202407]
12. Watson PG, Young RD. Scleral structure, organisation and disease. A review Exp Eye Res 2004;78:609–623.
13. Girard MJ, Downs JC, Burgoyne CF, Suh JK. Peripapillary and posterior scleral mechanics-part I: development of an anisotropic hyperelastic constitutive model. J Biomech Eng 2009;131:051011. [PubMed: 19388781]
14. Sigal IA, Flanagan JG, Ethier CR. Factors influencing optic nerve head biomechanics. Invest Ophthalmol Vis Sci 2005;46:4189–4199. [PubMed: 16249498]
15. Rochtchina E, Mitchell P, Wang JJ. Relationship between age and intraocular pressure: the Blue Mountains Eye Study. Clin Experiment Ophthalmol 2002;30:173–175. [PubMed: 12010208]
16. Nomura H, Ando F, Niino N, Shimokata H, Miyake Y. The relationship between age and intraocular pressure in a Japanese population: the influence of central corneal thickness. Curr Eye Res 2002;24:81–85. [PubMed: 12187477]
17. Nomura H, Shimokata H, Ando F, Miyake Y, Kuzuya F. Age-related changes in intraocular pressure in a large Japanese population: a cross-sectional and longitudinal study. Ophthalmology 1999;106:2016–2022. [PubMed: 10519601]
18. Weih LM, Mukesh BN, McCarty CA, Taylor HR. Association of demographic, familial, medical, and ocular factors with intraocular pressure. Arch Ophthalmol 2001;119:875–880. [PubMed: 11405839]
19. Klein BE, Klein R, Linton KL. Intraocular pressure in an American community. The Beaver Dam Eye Study. Invest Ophthalmol Vis Sci 1992;33:2224–2228. [PubMed: 1607232]
20. Leske MC, Connell AM, Wu SY, Hyman L, Schachat AP. Distribution of intraocular pressure. The Barbados Eye Study. Arch Ophthalmol 1997;115:1051–1057. [PubMed: 9258228]
21. Wu SY, Leske MC. Associations with intraocular pressure in the Barbados Eye Study. Arch Ophthalmol 1997;115:1572–1576. [PubMed: 9400792]
22. Drance SM, Sweeney VP, Morgan RW, Feldman F. Studies of factors involved in the production of low tension glaucoma. Arch Ophthalmol 1973;89:457–465. [PubMed: 4706442]
23. Levene RZ. Low tension glaucoma: a critical review and new material. Surv Ophthalmol 1980;24:621–664. [PubMed: 7414505]
24. Chumbley LC, Brubaker RF. Low-tension glaucoma. Am J Ophthalmol 1976;81:761–767. [PubMed: 937430]
25. Goldberg I, Hollows FC, Kass MA, Becker B. Systemic factors in patients with low-tension glaucoma. Br J Ophthalmol 1981;65:56–62. [PubMed: 7448157]
26. Klein BE, Klein R, Sponsel WE, et al. Prevalence of glaucoma. The Beaver Dam Eye Study. Ophthalmology 1992;99:1499–1504. [PubMed: 1454314]
27. Geijssen, HC. Studies on normal pressure glaucoma. Amstelveen: Kugler Publications; 1991.
28. Tielsch JM, Sommer A, Katz J, Royall RM, Quigley HA, Javitt J. Racial variations in the prevalence of primary open-angle glaucoma. The Baltimore Eye Survey. Jama 1991;266:369–374. [PubMed: 2056646]
29. Gordon MO, Beiser JA, Brandt JD, et al. The Ocular Hypertension Treatment Study: baseline factors that predict the onset of primary open-angle glaucoma. Arch Ophthalmol 2002;120:714–720. discussion 829–730. [PubMed: 12049575]
30. Nouri-Mahdavi K, Hoffman D, Coleman AL, et al. Predictive factors for glaucomatous visual field progression in the Advanced Glaucoma Intervention Study. Ophthalmology 2004;111:1627–1635. [PubMed: 15350314]
31. Heijl A, Leske MC, Bengtsson B, Bengtsson B, Hussein M. Measuring visual field progression in the Early Manifest Glaucoma Trial. Acta Ophthalmol Scand 2003;81:286–293. [PubMed: 12780410]

32. Albon J, Karwatowski WS, Easty DL, Sims TJ, Duance VC. Age related changes in the non-collagenous components of the extracellular matrix of the human lamina cribrosa. Br J Ophthalmol 2000;84:311–317. [PubMed: 10684844]
33. Albon J, Karwatowski WS, Avery N, Easty DL, Duance VC. Changes in the collagenous matrix of the aging human lamina cribrosa. Br J Ophthalmol 1995;79:368–375. [PubMed: 7742286]
34. Hernandez MR, Luo XX, Andrzejewska W, Neufeld AH. Age-related changes in the extracellular matrix of the human optic nerve head. Am J Ophthalmol 1989;107:476–484. [PubMed: 2653045]
35. Bailey AJ, Paul RG, Knott L. Mechanisms of maturation and ageing of collagen. Mech Ageing Dev 1998;106:1–56. [PubMed: 9883973]
36. Spoerl E, Boehm AG, Pillunat LE. The influence of various substances on the biomechanical behavior of lamina cribrosa and peripapillary sclera. Invest Ophthalmol Vis Sci 2005;46:1286–1290. [PubMed: 15790892]
37. Siegwart JT Jr, Norton TT. Regulation of the mechanical properties of tree shrew sclera by the visual environment. Vision Res 1999;39:387–407. [PubMed: 10326144]
38. Avetisov ES, Savitskaya NF, Vinetskaya MI, Iomdina EN. A study of biochemical and biomechanical qualities of normal and myopic eye sclera in humans of different age groups. Metab Pediatr Syst Ophthalmol 1983;7:183–188. [PubMed: 6678372]
39. Curtin BJ. Physiopathologic aspects of scleral stress-strain. Trans Am Ophthalmol Soc 1969;67:417–461. [PubMed: 5381306]
40. Friberg TR, Lace JW. A comparison of the elastic properties of human choroid and sclera. Exp Eye Res 1988;47:429–436. [PubMed: 3181326]
41. Downs JC, Suh JK, Thomas KA, Bellezza AJ, Burgoyne CF, Hart RT. Viscoelastic characterization of peripapillary sclera: material properties by quadrant in rabbit and monkey eyes. J Biomech Eng 2003;125:124–131. [PubMed: 12661206]
42. Downs JC, Suh JK, Thomas KA, Bellezza AJ, Hart RT, Burgoyne CF. Viscoelastic material properties of the peripapillary sclera in normal and early-glaucoma monkey eyes. Invest Ophthalmol Vis Sci 2005;46:540–546. [PubMed: 15671280]
43. Girard M, Suh JK, Hart RT, Burgoyne CF, Downs JC. Effects of storage time on the mechanical properties of rabbit peripapillary sclera after enucleation. Curr Eye Res 2007;32:465–470. [PubMed: 17514532]
44. Girard MJ, Downs JC, Burgoyne CF, Suh JK. Experimental surface strain mapping of porcine peripapillary sclera due to elevations of intraocular pressure. J Biomech Eng 2008;130:041017. [PubMed: 18601459]
45. Girard MJ, Downs JC, Bottlang M, Burgoyne CF, Suh JK. Peripapillary and Posterior Scleral Mechanics-Part II: Experimental and Inverse Finite Element Characterization. J Biomech Eng 2009;131:051012. [PubMed: 19388782]
46. Pinsky PM, van der Heide D, Chernyak D. Computational modeling of mechanical anisotropy in the cornea and sclera. J Cataract Refract Surg 2005;31:136–145. [PubMed: 15721706]
47. Nguyen TD, Jones RE, Boyce BL. A nonlinear anisotropic viscoelastic model for the tensile behavior of the corneal stroma. J Biomech Eng 2008;130:041020. [PubMed: 18601462]
48. Driessen NJ, Peters GW, Huyghe JM, Bouten CV, Baaijens FP. Remodelling of continuously distributed collagen fibres in soft connective tissues. J Biomech 2003;36:1151–1158. [PubMed: 12831741]
49. Gasser TC, Ogden RW, Holzapfel GA. Hyperelastic modelling of arterial layers with distributed collagen fibre orientations. J R Soc Interface 2006;3:15–35. [PubMed: 16849214]
50. Kroon M, Holzapfel GA. A new constitutive model for multi-layered collagenous tissues. J Biomech. 2008
51. Tigges J, Gordon TP, McClure HM, Hall EC, Peters A. Survival rate and life span of rhesus monkeys at the Yerkes regional primate research center. American Journal of Primatology 1988;15:263–273.
52. Erne OK, Reid JB, Ehmke LW, Sommers MB, Madey SM, Bottlang M. Depth-dependent strain of patellofemoral articular cartilage in unconfined compression. J Biomech 2005;38:667–672. [PubMed: 15713286]

53. Kessler O, Lacatusu E, Sommers MB, Mayr E, Bottlang M. Malrotation in total knee arthroplasty: effect on tibial cortex strain captured by laser-based strain acquisition. Clin Biomech (Bristol, Avon) 2006;21:603–609.
54. Bellezza AJ, Rintalan CJ, Thompson HW, Downs JC, Hart RT, Burgoyne CF. Deformation of the lamina cribrosa and anterior scleral canal wall in early experimental glaucoma. Invest Ophthalmol Vis Sci 2003;44:623–637. [PubMed: 12556392]
55. Downs JC, Yang H, Girkin C, et al. Three-dimensional histomorphometry of the normal and early glaucomatous monkey optic nerve head: neural canal and subarachnoid space architecture. Invest Ophthalmol Vis Sci 2007;48:3195–3208. [PubMed: 17591889]
56. Fisher, NI. Statistical analysis of circular data. Cambridge, UK: Cambridge University Press; 1993.
57. Fung, YC. Biomechanics: Mechanical properties of living tissues. 2. New York, NY: Springer-Verlag; 1993.
58. Woo SL, Kobayashi AS, Schlegel WA, Lawrence C. Nonlinear material properties of intact cornea and sclera. Exp Eye Res 1972;14:29–39. [PubMed: 5039845]
59. Phillips JR, McBrien NA. Form deprivation myopia: elastic properties of sclera. Ophthalmic Physiol Opt 1995;15:357–362. [PubMed: 8524554]
60. Wollensak G, Spoerl E. Collagen crosslinking of human and porcine sclera. J Cataract Refract Surg 2004;30:689–695. [PubMed: 15050269]
61. Olesen, CG.; Tertinegg, I.; Eilaghi, A., et al. Measuring the biaxial stress-strain characteristics of the human sclera. Proceedings of the ASME, Summer Bioengineering Conference; Keystone, Colorado, USA. 2007;
62. Weiyi C, Wang X, Wang C, Tao L, Li X, Zhang Q. An experimental study on collagen content and biomechanical properties of sclera after posterior sclera reinforcement. Clin Biomech (Bristol, Avon) 2008;23(Suppl 1):S17–20.
63. Schultz DS, Lotz JC, Lee SM, Trinidad ML, Stewart JM. Structural Factors That Mediate Scleral Stiffness. Invest Ophthalmol Vis Sci 2008;42:4232–4236. [PubMed: 18539943]
64. Weiss JA, Maker BN, Govindjee S. Finite element implementation of incompressible, transversely isotropic hyperelasticity. Comput Methods Appl Mech Engrg 1996;135:107–128.
65. Olberding JE, Suh J-KF. A dual optimization method for the material parameter identification of a biphasic poroviscoelastic hydrogel: Potential application to hypercompliant soft tissues. J Biomech 2006;39:2468–2475. [PubMed: 16153650]
66. Price, KV.; Storn, RM.; Lampinen, JA. Differential evolution. A practical approach to global optimization. Berlin: Germany Springer; 2005.
67. Downs JC, Ensor ME, Bellezza AJ, Thompson HW, Hart RT, Burgoyne CF. Posterior scleral thickness in perfusion-fixed normal and early-glaucoma monkey eyes. Invest Ophthalmol Vis Sci 2001;42:3202–3208. [PubMed: 11726623]
68. Jackson TL, Hussain A, Hodgetts A, et al. Human scleral hydraulic conductivity: age-related changes, topographical variation, and potential scleral outflow facility. Invest Ophthalmol Vis Sci 2006;47:4942–4946. [PubMed: 17065511]
69. Vannas S, Teir H. Observations on structures and age changes in the human sclera. Acta Ophthalmol (Copenh) 1960;38:268–279. [PubMed: 13855196]
70. McBrien NA, Cornell LM, Gentle A. Structural and ultrastructural changes to the sclera in a mammalian model of high myopia. Invest Ophthalmol Vis Sci 2001;42:2179–2187. [PubMed: 11527928]
71. Burgoyne CF, Downs JC. Premise and Prediction-How Optic Nerve Head Biomechanics Underlies the Susceptibility and Clinical Behavior of the Aged Optic Nerve Head. J Glaucoma 2008;17:318–328. [PubMed: 18552618]
72. Downs JC, Roberts MD, Burgoyne CF. Mechanical environment of the optic nerve head in glaucoma. Optom Vis Sci 2008;85:425–435. [PubMed: 18521012]
73. Kokott W. Das spaltlinienbild der sklera. (Ein beitrag zum funktionellen bau der sklera). Klin Mbl Augen 1934;92:177–185.
74. Hernandez MR, Luo XX, Igoe F, Neufeld AH. Extracellular matrix of the human lamina cribrosa. Am J Ophthalmol 1987;104:567–576. [PubMed: 3318474]

75. Greene PR. Mechanical considerations in myopia: relative effects of accommodation, convergence, intraocular pressure, and the extraocular muscles. Am J Optom Physiol Opt 1980;57:902–914. [PubMed: 7223834]
76. Zulliger MA, Fridez P, Hayashi K, Stergiopulos N. A strain energy function for arteries accounting for wall composition and structure. Journal of Biomechanics 2004;37:989–1000. [PubMed: 15165869]
77. Weiss JA, Gardiner JC. Computational modeling of ligament mechanics. Crit Rev Biomed Eng 2001;29:303–371. [PubMed: 11730098]
78. Yamaoka A, Matsuo T, Shiraga F, Ohtsuki H. TIMP-1 production by human scleral fibroblast decreases in response to cyclic mechanical stretching. Ophthalmic Res 2001;33:98–101. [PubMed: 11244355]
79. Cui W, Bryant MR, Sweet PM, McDonnell PJ. Changes in gene expression in response to mechanical strain in human scleral fibroblasts. Exp Eye Res 2004;78:275–284. [PubMed: 14729359]
80. Shelton L, Rada JS. Effects of cyclic mechanical stretch on extracellular matrix synthesis by human scleral fibroblasts. Exp Eye Res 2007;84:314–322. [PubMed: 17123515]
81. Fujikura H, Seko Y, Tokoro T, Mochizuki M, Shimokawa H. Involvement of mechanical stretch in the gelatinolytic activity of the fibrous sclera of chicks, in vitro. Jpn J Ophthalmol 2002;46:24–30. [PubMed: 11853710]
82. Albon J, Purslow PP, Karwatowski WS, Easty DL. Age related compliance of the lamina cribrosa in human eyes. Br J Ophthalmol 2000;84:318–323. [PubMed: 10684845]
83. Morrison JC, L'Hernault NL, Jerdan JA, Quigley HA. Ultrastructural location of extracellular matrix components in the optic nerve head. Arch Ophthalmol 1989;107:123–129. [PubMed: 2910271]
84. Quigley HA. Childhood glaucoma: results with trabeculotomy and study of reversible cupping. Ophthalmology 1982;89:219–226. [PubMed: 7088505]
85. Albon J, Farrant S, Akhtar S, et al. Connective tissue structure of the tree shrew optic nerve and associated ageing changes. Invest Ophthalmol Vis Sci 2007;48:2134–2144. [PubMed: 17460272]
86. Kotecha A, Izadi S, Jeffery G. Age-related changes in the thickness of the human lamina cribrosa. Br J Ophthalmol 2006;90:1531–1534. [PubMed: 16943226]
87. Greene PR, McMahon TA. Scleral creep vs. temperature and pressure in vitro. Exp Eye Res 1979;29:527–537. [PubMed: 527689]
88. Rigby BJ, Hirai N, Spikes JD, Eyring H. The Mechanical Properties of Rat Tail Tendon. J Gen Physiol 1959;43:265–283. [PubMed: 19873525]
89. Woo SL, Lee TQ, Gomez MA, Sato S, Field FP. Temperature dependent behavior of the canine medial collateral ligament. J Biomech Eng 1987;109:68–71. [PubMed: 3560883]
90. Holzapfel G, Gasser T, Ogden R. A New Constitutive Framework for Arterial Wall Mechanics and a Comparative Study of Material Models. Journal of Elasticity 2000;61:1–48.
91. Rezakhaniha R, Stergiopulos N. A structural model of the venous wall considering elastin anisotropy. J Biomech Eng 2008;130:031017. [PubMed: 18532866]
92. Roberts, MD.; Hart, RT.; Liang, Y.; Bellezza, AJ.; Burgoyne, CF.; Downs, JC. Continuum-level finite element modeling of the optic nerve head using a fabric tensor based description of the lamina cribrosa. Proceedings of the ASME, Summer Bioengineering Conference; Keystone, Colorado, USA. 2007;
93. Downs, JC.; Roberts, MD.; Burgoyne, CF.; Hart, RT. Finite element modeling of the lamina cribrosa microarchitecture in the normal and early glaucoma optic nerve head. Proceedings of the ASME, Summer Bioengineering Conference; Keystone, Colorado, USA. 2007;
94. Kokott W. Über mechanisch-funktionelle Strukturen des Auges. Graefe's Archive for Clinical and Experimental Ophthalmology 1938;138:424–485.
95. Komai Y, Ushiki T. The three-dimensional organization of collagen fibrils in the human cornea and sclera. Invest Ophthalmol Vis Sci 1991;32:2244–2258. [PubMed: 2071337]

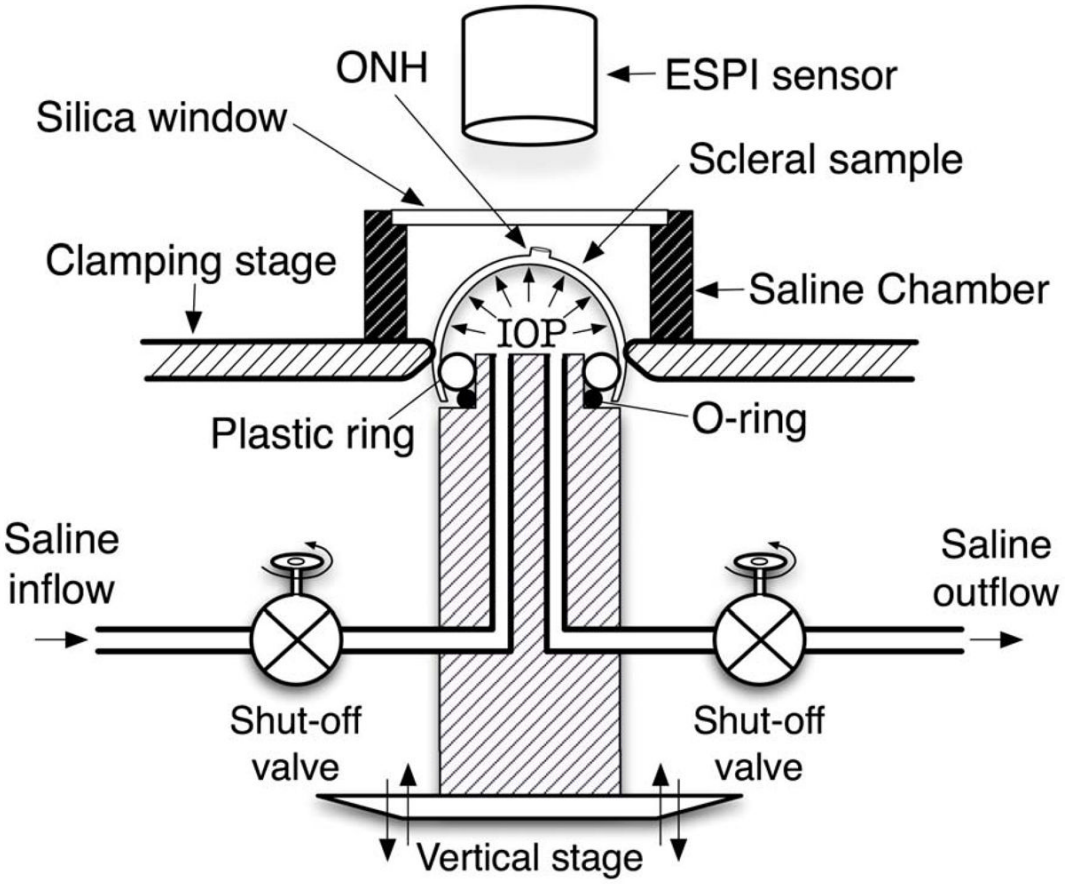

Figure 1.
Schematic of the scleral shell pressurization apparatus. The posterior scleral shell was first mounted onto the plastic ring, and then clamped slightly above the equator by moving the vertical stage toward the clamping stage. Saline outflow was interrupted after saline filled the posterior shell cavity and IOP reached 5 mmHg. The scleral surface was imaged with an electronic speckle pattern interferometry (ESPI) sensor as IOP increased from 5 to 45 mmHg in 0.2 mmHg increments.

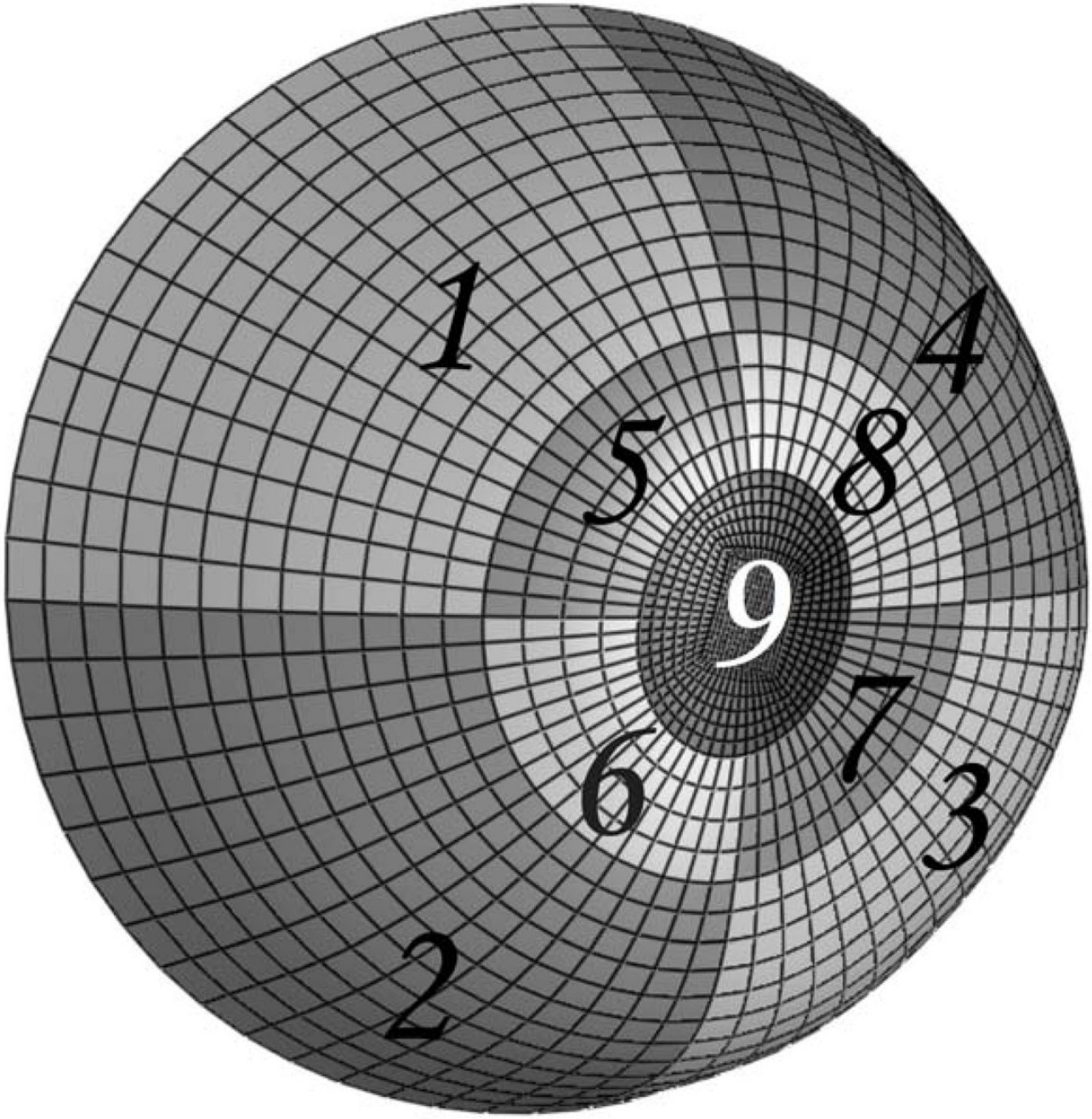

Figure 2.
Anatomically accurate geometry of one posterior scleral shell (from the clamping boundary to the ONH) that was reconstructed from experimental topography and thickness measurements. Regions 1–4 encompass the peripheral sclera, Regions 5–8 the peripapillary sclera and Region 9 the ONH. The peripapillary sclera (Regions 5–8) extended approximately 1.5 to 1.7 mm from the scleral canal, which was defined as the border between the ONH (Region 9) and the peripapillary sclera (Regions 5–8). The clamping ring was located approximately 3 mm posterior to the equator.

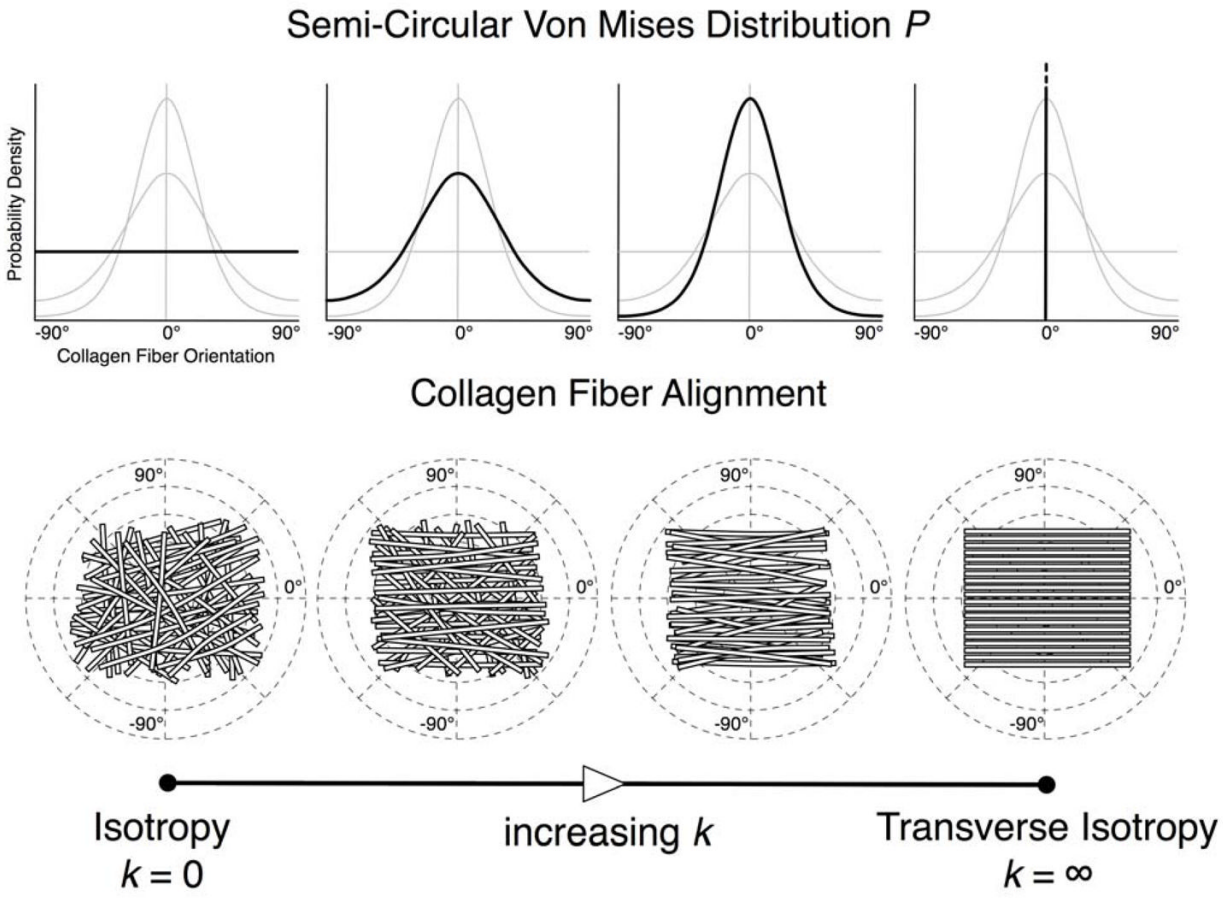

Figure 3.

Semi-circular von-Mises distribution describing local collagen fiber alignment. As the fiber concentration factor k increases, collagen fibers become more aligned along the preferred fiber orientation ($\theta_p = 0°$ in this example). When $k = 0$, collagen fibers are randomly organized, resulting in equal stiffness in all orientations (relevant to skin tissue). This material symmetry is known as planar isotropy. When $k = \infty$, collagen fibers are all oriented in a particular preferred orientation, which creates high stiffness along θ_p and high compliance perpendicular to θ_p (relevant to tendons and ligaments). This material symmetry is known as transverse isotropy.

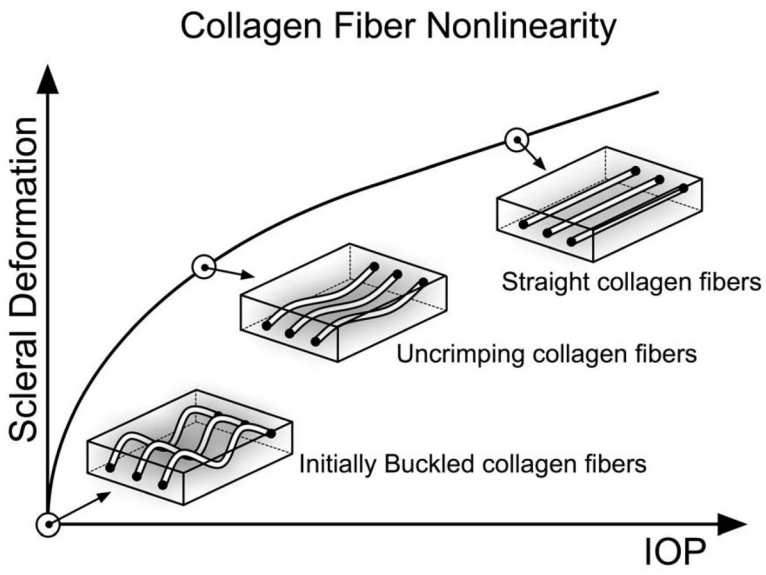

Figure 4.
Uncrimping of the collagen fibers induces scleral stiffening at the macroscopic level. Initially the collagen fibers are buckled, then uncrimp and eventually become straight due to acute elevations of IOP, thus limiting scleral deformations at high IOP values. Note that the parameters c_3 and c_4 govern the degree of nonlinearity of each scleral shell.

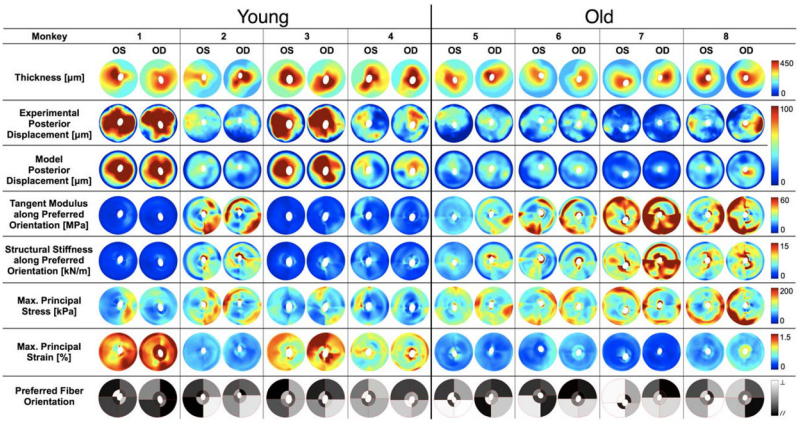

Figure 5.

Individual results for all posterior scleral shells as viewed from the back of the eye (Superior is up). Scleral thickness was experimentally measured at IOP = 5 mmHg and interpolated to obtain continuous thickness maps. Tangent modulus, structural stiffness, maximum principal stress and strain are shown for all eyes at a single IOP of 30 mmHg. Good agreement is observed between FE-computed and experimentally measured posterior displacements (plotted for an IOP range of 5–30 mmHg). Finally the preferred fiber orientation is shown for all eight regions of each eye, where // (black) corresponds to a collagen fiber organization tangent to the scleral canal (circumferential, $\theta_p = 0°$) and ⊥ (white, $\theta_p = 90°$) corresponds to a fiber organization that is perpendicular to the scleral canal (meridional). Note that the data for the two eyes of each monkey are much more similar than between monkeys, and there are clear age-related differences in all measures except for preferred collagen fiber orientation.

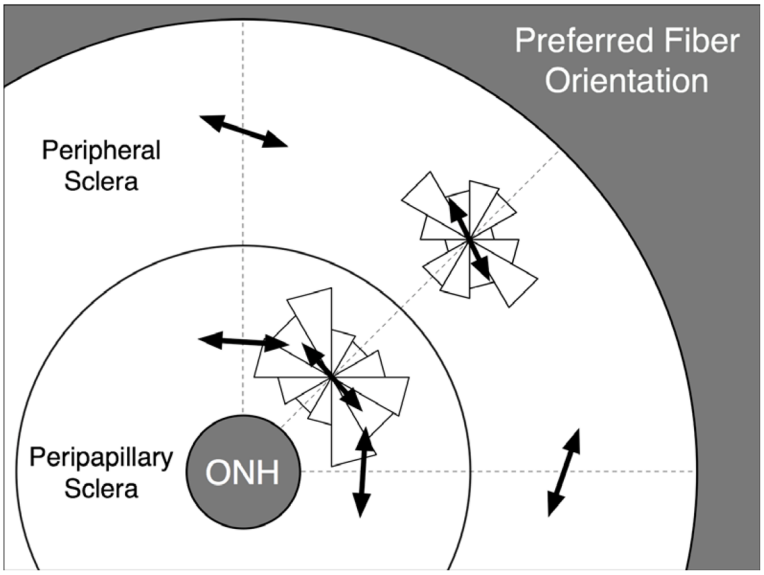

Figure 6.

Pooled distributions (all eyes) of the preferred fiber orientation in both the peripapillary and peripheral scleral regions are shown as two symmetric rose diagrams, in which larger triangles indicate the most commonly derived orientations. Mean preferred fiber orientations (black arrows) were computed for each of both distributions using a circular statistics formula[56] and were equal to 176.2° and 162.0° in the peripapillary and peripheral sclera, respectively. Note that 0° or 180° correspond to an orientation tangent to the scleral canal and 90° to an orientation perpendicular to the scleral canal. On average, this result suggests a tendency toward a circumferential organization of the collagen fibers around the scleral canal in both the peripapillary and the peripheral sclera.

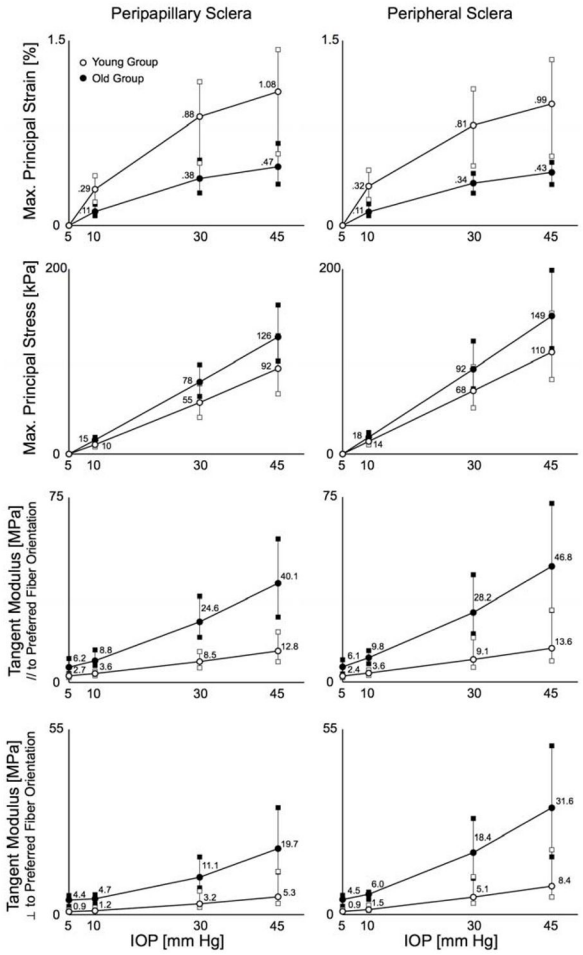

Figure 7.

Maximum principal strain, maximum principal stress, and tangent moduli distributions (error bars show the 25th, 50th, and 75th percentiles) plotted by age group for both scleral regions (peripapillary and peripheral) at the following IOPs: 5, 10, 30 and 45 mmHg. On average, sclera from the old monkeys exhibited higher tangent moduli and stress, but lower strain than that from the young monkeys. Note the nonlinear relationship between IOP and strain, which is due to the increase of tangent moduli with IOP (the sclera stiffens as IOP increases).

Table 1

Estimated model parameters (c_1, c_3, c_4, k_1 and k_2) from inverse FE simulations. Data are shown for both eyes of each monkey in both the young and old groups. Note that all eight other model parameters for each eye (the preferred fiber orientations) are shown in the last row of Figure 5.

Young Sclera	Monkey	1		2		3		4	
	Sex	M		M		M		M	
	Age [years]	0.5		1.7		1.7		2.1	
	Eye	os	od	os	od	os	od	os	od
	c_1 [kPa]	116	63	782	629	200	192	197	100
	c_3 [kPa]	26.6	19.4	3.42	2.16	14.8	21.2	6.19	15.6
	c_4 [−]	280	273	1344	1574	325	362	602	505
	k_1 [−]	1.56	1.37	1.98	1.65	1.28	2.67	2.25	1.40
	k_2 [−]	1.67	3.14	1.49	2.99	1.84	3.61	2.65	4.57

Old Sclera	Monkey	5		6		7		8	
	Sex	M		F		M		F	
	Age [years]	18.0		20.3		23.0		30.3	
	Eye	os	od	os	od	os	od	os	od
	c_1 [kPa]	1290	1191	2039	964	1520	2722	643	232
	c_3 [kPa]	61.9	7.41	2.38	1.60	6.19	4.16	4.21	5.82
	c_4 [−]	463	1236	1703	1583	1717	2934	1345	1390
	k_1 [−]	1.40	1.15	4.99	1.62	1.20	2.04	1.50	2.10
	k_2 [−]	2.67	1.49	0.39	4.99	3.84	3.00	2.23	5.78